Design of a Highly-Integrated W-Band Up-Down Frequency Converter

Vladimir Marinov, Dr. Ben Kieniewicz, Nicolo Fasciano, Bertie Kemp, Dr. Sidina Wane,
EECL, London, UK
vlad@euroecl.com, info@euroecl.com
www.eecl.co.uk

Proceedings of the Automated Radio Frequency and Microwave Measurement Society (ARMMS) Conference, April 2025

***Abstract*— W-band frequencies (71 GHz - 86 GHz) have seen a significant rise in interest, driven by applications such as automotive radar, satellite communications, and high-capacity mobile networks. This has resulted in an increase in demand for test equipment in this band, with a particular focus on highly integrated, lower-cost solutions.**

This paper presents the design of an up-down frequency converter from K-band to W-band, with a shared local oscillator (LO) enabling coherent (frequency-and-phase-locked) up-down conversion. The design also includes Built-in Self Test (BIST) functionality, featuring an internal self-test loopback mode and output power measurement. The converter utilizes heater temperature stabilization for long-term, calibrated performance and verification in a wide-range of operating environments.

In conjunction with a DC to K-band Dual Channel Frequency Extender developed by EECL, a modular system is created to extend low-frequency test equipment capabilities up to W-Band. The system was initially developed for production-line testing of automotive radar chips, but is also suitable for other applications, such as W-band radar frontends, spectrum analyzer extenders, and VNA extenders.

I. Introduction

The W-band portion of the electromagnetic spectrum (75 GHz-110 GHz) has seen a massive increase in interest over the past years. It has become the de facto standard for automotive radar applications [1], and has seen increasing interest for future high-capacity 5G and 6G networks [2], as well as high-capacity satellite communications [3].

This, in turn, increases the requirements for test and measurement systems operating in this frequency band. Traditional measurement instruments, such as Vector Network Analyzers and Spectrum Analyzers have been extended to support W-Band through the use of mixer extension heads. However, there remains a lack of equipment to generate, interact with or measure modulated wideband signals at these frequencies. Additionally, conventional test systems in this range are very costly, as they rely on expensive alumina substrates and chip-and-wire construction techniques. Integration of such test systems usually requires extensive uses of waveguide interconnects, further increasing complexity, cost, size, and mass.

This paper presents a new phase-frequency-locked, up-down frequency converter, enabling signal translation between K-Band and W-Band. By frequency converting signals from widely-avaialable K-Band test equipment, the module facilitates the generation and analysis of phase-sensitive wideband modulated signals at W-Band. The design achieves a very high level of integration, encapsulating bidirectional frequency conversion, amplification, DC biasing and control, and self-test functionality within a single module. The module is based on conventional printed circuit board (PCB) technologies, and integrates both surface mount and bare-die devices. The final module has dimensions of only $75 \times 75 \times 16\,\mathrm{mm}$ and consumes only $5.8\,\mathrm{W}$ under nominal operation.

The module is suitable for general use as a front-end for W-Band applications, such as automotive radar, spectrum analyzers or VNA extenders, and many other general purpose applications. The module is commercially available for purchase from EECL.

The rest of this paper is structured as follows: section II details the frequency converter architecture, section III details the module hardware implementation, and section IV presents experimentally measured results and achieved specifications. Section V demonstrates examples of using the converter for frequency extending lower-frequency VNAs to W-Band.

II. Converter Architecture

The high-level architecture overview for the converter can be seen in fig. 1, noting that some passive components such as image reject filters, LO splitter, and DC blocking capacitors have been ommited for clarity.

The converter can be broadly divided into three main subsections - a shared Local Oscillator (LO) section, a W-band upconversion section, and a W-band downconversion section.

The shared LO RF chain comprises amplification, a frequency doubler, and a bandpass filter. The input LO frequency (nominally $25\,\mathrm{GHz}$ to $30\,\mathrm{GHz}$) is doubled internally, allowing the input LO to be K-band, same as the IF input and outputs. The doubled LO is amplified, split to the upconversion and downconversion mixers through a printed power divider, and then further amplified to the correct mixer drive level. The integrated amplification inside the LO chain allows the module input LO drive level to be only $-12\,\mathrm{dBm}$ - much lower than many commercially available frequency converters at these frequencies, many of which require upwards of $10\,\mathrm{dBm}$ to $15\,\mathrm{dBm}$ of input LO power.

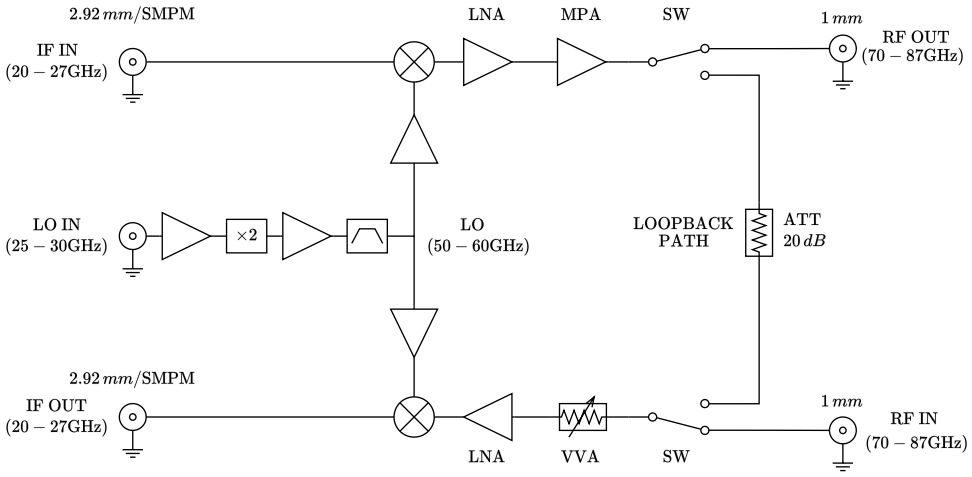

Fig. 1. High-Level Converter Architecture

A printed bandpass filter is used to supress any non-doubled input LO signals (25 GHz to 30 GHz) from reaching the mixer, creating unwanted conversion products.

The shared-LO nature of the up-down-conversion guarantees a stable phase relationship between the IF input and outputs, thus allowing the converter to be used in phase-sensitive applications, such as VNA extenders, and radar front-ends.

The upconversion RF chain consists of the upconverting mixer and two amplification stages - a W-Band Low-Noise Amplifier (LNA) and a W-Band Medium Power Amplifier (MPA). This allows for a high typical upconversion gain of 15 dB and maximum output power of 14 dBm at 77 GHz.

The downconverter RF chain consists of an input Voltage-Variable Attenuator (VVA) followed a W-Band LNA identical to the one used in the upconversion chain. The variable attenuator allows flexible configuration of the downconversion, supporting either a high maximum input power (up to 30 dBm) or a low noise figure (as low as 8 dB). Intermediate configurations are also possible, allowing the end user to tailor input power handling and noise performance to their application requirements.

Since this converter was initially designed for long-term integration inside an industrial testing environment, a key consideration was the addition of Built-in Self-Test functionality, to allow for the device performance and health to be verified remotely and automatically.

The main such self-test feature is a switchable internal loopback connection (see fig. 1) that allows for full performance validation, without requiring the converter to be disconnected from a DUT or associated test fixture. A fixed 20 dB attenuator is present in the loopback path to allow self-test even at the maximum upconversion output power without adjusting the downconversion VVA settings.

Additional built-in self-test functionality includes an output RF power detector integrated in the upconversion chain, and a suite of monitoring features on all associated DC circuitry, including precision RF supply voltage monitoring and bias current measurement.

These features allow a comprehensive automatic performance verification, with minimal system downtime, and no manual intervention.

III. Hardware Implementation

The final assembled prototype module, representing the physical hardware implementation of the proposed architecture, is shown in fig. 2.

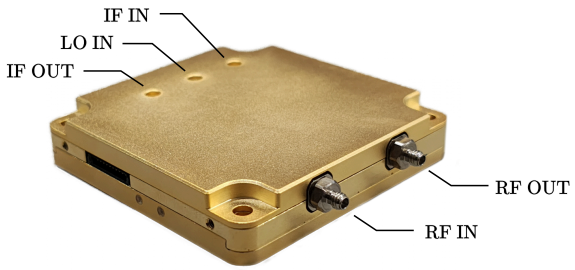

Fig. 2. Final Prototype Assembly

The module implements a multi-board approach, where the main RF printed circuit board (PCB) is supplemented by a separate DC Bias and Control board. An exploded view of the full multi-board assembly can be seen in fig. 3.

The main RF PCB is based on a 127 µm Rogers RT-5880 substrate which is post-bonded on a metal carrier. This serves to mechanically and thermaly stabilize the thin RF substrate. To mitigate the long lead-time of commercial metal-backed RF PCB suppliers, the bonding of the board and carrier was done in house using based on a custom-developed process.

A. Die-on-Board Devices and Wirebonding

Despite the active ongoing research into packaging MMICs at E-Band and W-Band frequencies [4], [5], most devices operating in this frequency range (including all active devices

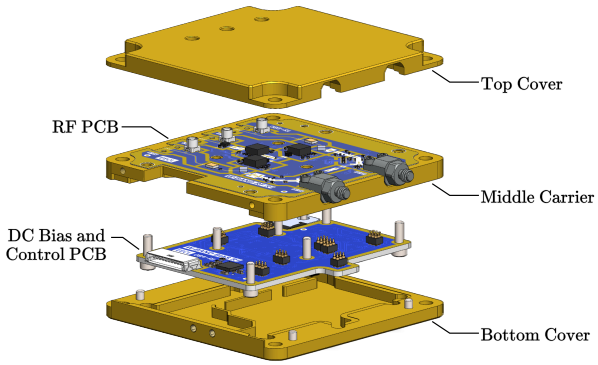

Fig. 3. Multi-Board Assembly - Exploded View

used in the upconversion and downconversion RF chains of this converter) are only avaialbe in bare-die form, due to the significant complications of package-induced parasitics. Significant design effort and care was taken to correctly integrate these devices into the overall PCB design, and to allow for board assembly that includes both traditional surface mount (SMT) components, as well as the aforementioned bare die devices.

The bare-die MMIC devices in this converter are placed inside precision laser-cut cavities in the RF PCB, and are thus mounted directly to the middle metal carrier, using silver epoxy. This eliminates the thermal interface of the board dielectric, thus significantly improving device cooling. This is crucial, since the bare-die amplifiers can dissipate significant power. For example, the medium-power amplifier in the upconversion RF chain (see fig. 1) dissipates on the order of $1.5\,\mathrm{W}$ inside of a die that measures $5.7\,\mathrm{mm}^2$. A diagram showing the cross-section of the aforementioned cutout can be seen in fig. 4.

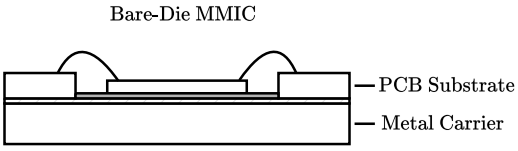

Fig. 4. Cross-sectional view of MMIC integrated within laser-cut PCB cavity

The connections (both RF and DC) of the bare-die devices to the PCB were implemented using $25\,\mu\mathrm{m}$ diameter gold wirebonds. The correct design of the RF connection is critical, due to parasitic reactance introduced by the wirebond, dominated by an inductance of approximately $1\,\mathrm{pH}$ per $1\,\mu\mathrm{m}$ of bond length. For a $300\,\mu\mathrm{m}$ wirebond length, as used in this design, this corresponds to a *return* loss on the order of $3.5\,\mathrm{dB}$ in the desired frequency range. This is clearly unusable for any practical applications.

Thus, the wirebond must be compensated, through an appropriate impedance matching circuit. For this design, an LC impedance matching circuit was used, which was implemented in a distributed fashion on the microstrip transmission lines leading into each MMIC. Two wire bonds, in the well-established RF V-bond configuration [6], are used for each RF MMIC connection. A diagram of the distributed matching section and associated bond wires are shown in fig. 5.

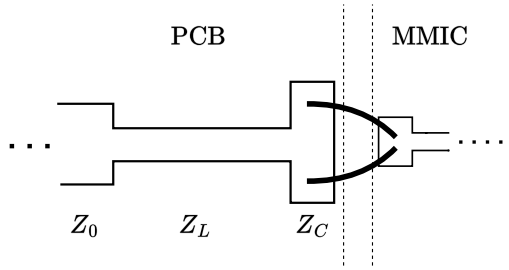

Fig. 5. V-Bond wirebonds with associated LC impedance matching circuit

The exact dimensions of the LC matching sections and associated wirebond parameters were empirically determined and optimized via 3D electromagnetic simulation. A comparison of the simulated compensated and uncompensated wire bond connections can be seen in fig. 6. The compensated wirebonds show a good resonant match, with a return loss better than $15\,\mathrm{dB}$ over the desired operating bandwidth.

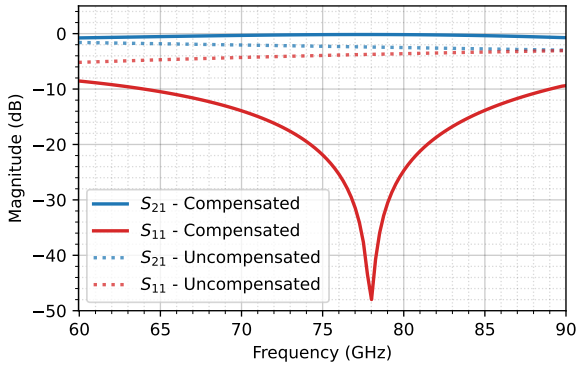

Fig. 6. S-Parameters of Uncompensated and Compensated RF wirebond connections

During assembly of the prototype, the die placement and wirebonding was completed entirely in-house, with the wirebonds implemented via a fine-tuned custom profile on a semi-automatic wirebonder. Microscope photographs of an integrated bare-die MMIC and associated wirebonds can be seen in fig. 7.

B. DC Bias Board and Active Biasing

A supplemental DC Bias and Control PCB is present in the converter, integrating all supporting functionality necessary for the RF system. It can be seen integrated into the module in fig. 8.

This board integrates all required DC power supply circuitry, a microcontroller for device configuration and

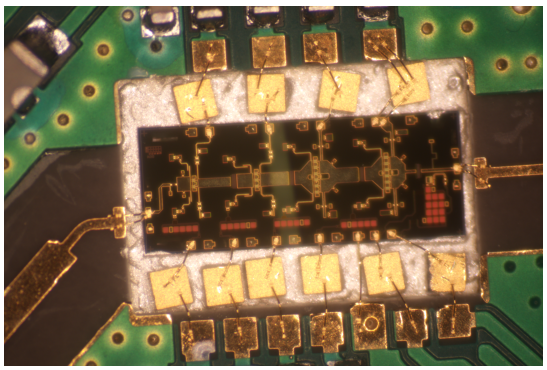

Fig. 7. Assembled bare-die and wire bonds

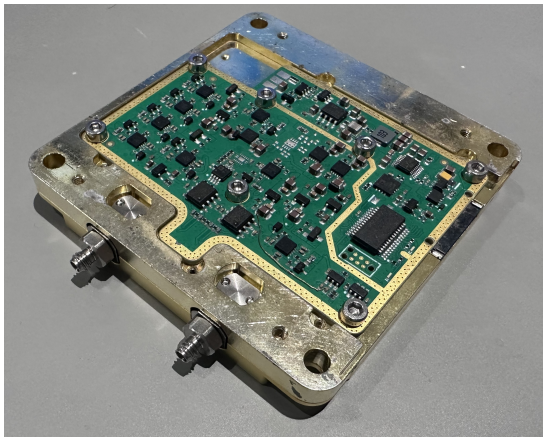

Fig. 8. DC Bias and Control board integrated in module

communication, and an active heater circuit that provides closed-loop temperature stabilization of the convereter module for long-term calibrated performance.

The DC Bias board also houses active bias blocks for each RF amplifier in the module. This ensures that bias current is independent of temperature and manufacturer variations, intrinsic in RF amplifiers. The active bias block is based on a proprietary op-amp circuit, optimized for minimal power dissipation, and stable drain current over device temperature and power supply variations.

C. Gasket Shielding and Absorber

Due to the high level of integration and dense physical layout of the proposed converter design, RF shielding gasket and Radiation-absorbent material (RAM) are neccessary to provide isolation between adjacent active devices, and supress any cavity resonant modes inside the module enclosure.

EECL's proprietary automated dispensing technology was used to integrate the shielding gasket and absorber material within the top metal case of the device. The completed cover can be seen in fig. 9.

The gasket allows for superior isolation between adjacent devices, thus optimizing channel isolation, gain flatness, and other key performance metrics. The absorber successfully removes any self-oscillations due to cavity-resonant feedback

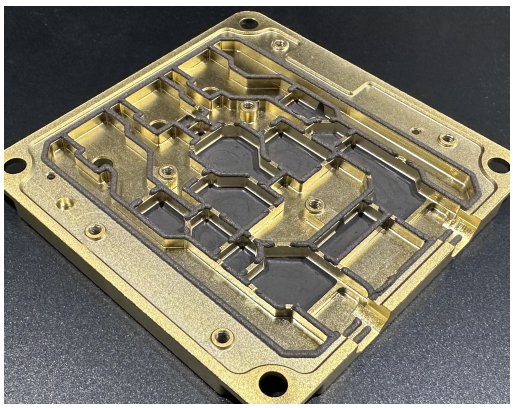

Fig. 9. Dispensed RF shielding gasket and absorber material

modes. This techonology is a key driver in enabling the dense integration and small size of the W-Band converter described in this paper, and is available as a commercial service from EECL.

IV. Results and Achieved Specifications

Initial testing of the prototype converter was performed with a Rohde & Schwarz FSVA3044 Spectrum Analyzer, extended to W-Band using the FS-Z90 harmonic mixer. A WR-12 to 1 mm adapter and 1 mm coaxial cable were used to connect the harmonic mixer to the W-Band Converter. To avoid compressing the FS-Z90 input, additional fixed waveguide attenuators were added in as neccessary, especially during P_{SAT} measurements. The measurement setup can be seen in fig. 10.

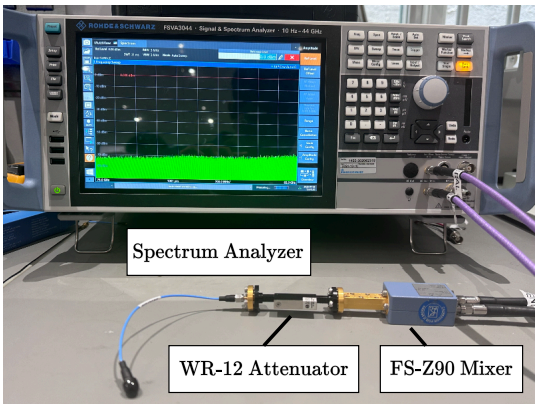

Fig. 10. Measurement setup for initial converter verification

This setup was used to characterize the upconversion chain, by injecting an IF signal of known frequency and power, and measuring the corresponding W-Band output signal. This technique was used to obtain measurements for the system upconversion gain, and upconversion saturated output power.

For all presented measurements, an input LO frequency of 27.5 GHz was used, corresponding to a doubled LO of 55 GHz and an output range of the converter of 75 GHz to 82 GHz. Other LO frequencies in the supported range

were also measured separately and provide similar overall performance, with the corresponding output frequency range shifted accordingly.

The upconversion gain S_{C21} of the module, measured at 30 frequency points, can be seen in fig. 11. The device offers significant conversion gain over the output frequency range, simplifying system integration for end users, and elimating the need for external amplification.

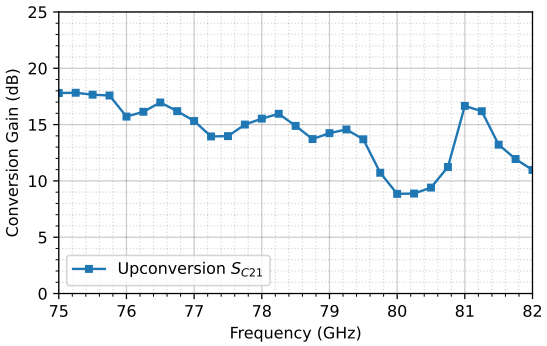

Fig. 11. Upconversion gain S_{C21} over frequency

The upconversion P_{SAT} (saturated output power) of the converter can be seen in fig. 12. The converter meets and exceeds the design requirement of $12\,\text{dBm}$, which was set out to allow the converter to be used for medium-power applications such as short-range radar frontends, for example for automotive applications.

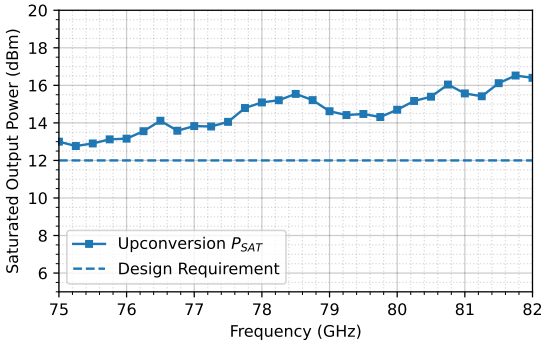

Fig. 12. Upconversion P_{SAT} (saturated output power) over frequency

The overall looped-back conversion gain of the device can also be measured, both with an external loopback (in the form of a short $1\,\text{mm}$ cable), or with the internal loopback enabled. This measurement was completed using a P5007A Keysight $44\,\text{GHz}$ VNA, and can be seen in fig. 13.

This measurement verifies that both the upconversion and downconversion chains are working as intended, and that the converter can perform simultaneous bidirectional frequency conversion. The internal (self-test) loopback path is also performing as intended, with an insertion loss of approximately $20\,\text{dB}$ as intended, allowing for safe self-test at maximum upconversion power output.

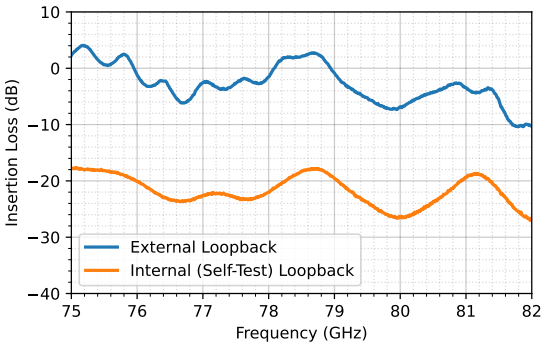

Fig. 13. Module looped-back conversion gain, with and without enabling internal self-test loopback path

V. VNA Extension Example

A key example use case of the W-Band frequency converter presented in this paper is to provide a low-cost method to extend lower-frequency test equipment, for example spectrum analyzers or vector network analyzers, to W-Band frequencies.

Two examples for VNA frequency extension are presented in this section. In the first example, the W-Band converter is used to directly extend a Keysight P5007A $44\,\text{GHz}$ VNA. In the second example, the W-Band converter is used in conjunction with EECL's existing DC to Ka-Band Dual Channel Frequency Extender, to extend a low-cost LA Techniques LA19-13-04B $8.5\,\text{GHz}$ VNA. Diagrams of both setups can be seen in fig. 14. Both measurement setups were configured to provide an example extended frequency range of $76\,\text{GHz}$ to $81\,\text{GHz}$.

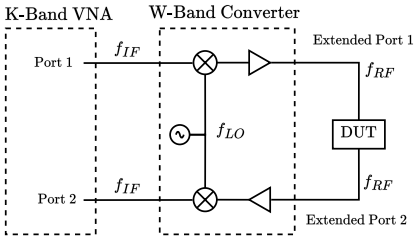

(a)

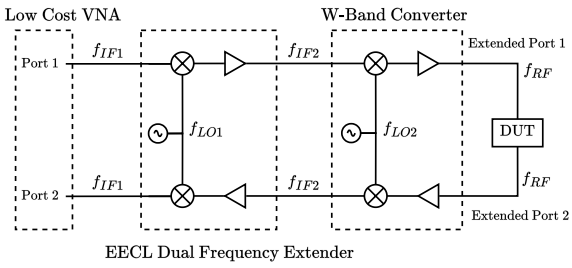

(b)

Fig. 14. VNA Extender Example setup diagrams. (a) $44\,\text{GHz}$ VNA direct extension, (b) $8.5\,\text{GHz}$ VNA extension including EECL Dual Frequency Extender

A picture of the second setup, including both EECL's Dual Frequency Extender and the W-Band converter can be seen in fig. 15.

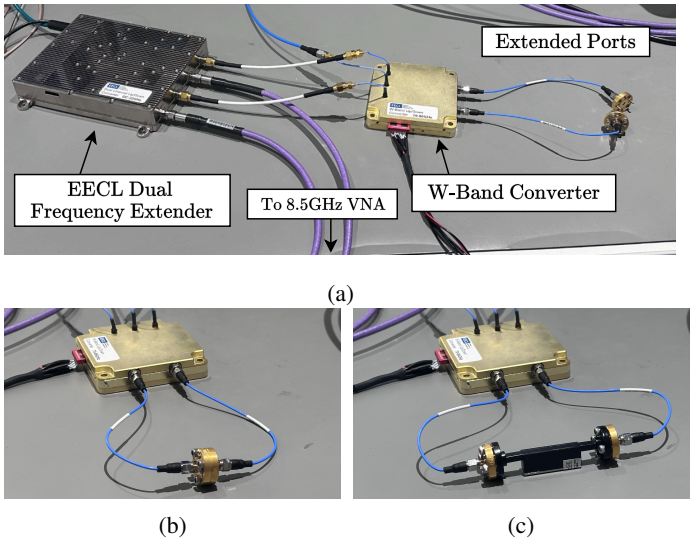

(a)

(b) (c)

Fig. 15. VNA Extender Measurements - (a) Second example setup with both EECL frequency converters, (b) Flush (Zero-length) Thru Calibration Measurement, (c) Attenuator DUT Measurement

Due to the phase-stable shared-LO nature of both the W-Band and Ka-Band converters, these system can be used to measure vector (magnitude *and* phase) S_{21} of a Device Under Test (DUT), however they cannot measure reflection coefficients (S_{11}, S_{22}) without the use of an external coupler. This, also means a full 2-port calibration (SOLT, TRL, etc.) cannot be performed on the extended S_{21} measurement. Instead, a Response calibration (also known as Normalization Thru calibration) is used, which yields sufficiently accurate results, provided that no significant reflection occurs at the various measurement interfaces. For waveguide measurements, such as the ones in this example, a true flush (or zero length) thru can be obtained for calibration by attaching the two waveguide ports directly to each other. For a more detailed description of response calibrations, and associated measurement uncertainty consult [7, p.195-196].

A $10\,\mathrm{dB}$ WR-12 waveguide attenuator S_{21} measurement was obtained and calibrated with both setups in the aforementioned manner. The flush (zero-length) thru calibration measurement, and DUT measurement connections can be seen in fig. 15. The resulting calibrated S_{21} measurements from both setups can be seen in fig. 16.

Both setups produce results with close agreement, and the measurements are consistent with the datasheet specifications for the attenuator. As part of future work, the authors aim to obtain a true measurement of the attenuator from a calibrated VNA and present a more representative comparison. Nevertheless, this measurement demonstrates that the converter can be used effectively as a VNA extender for vector S_{21} at W-Band frequencies.

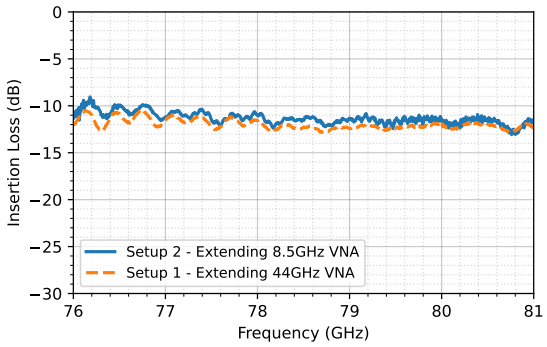

(a)

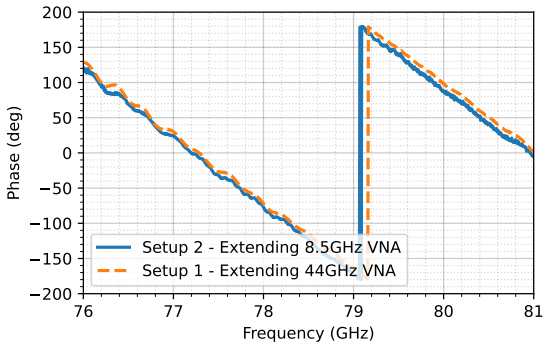

(b)

Fig. 16. Calibrated vector S_{21} measurement of $10\,\mathrm{dB}$ waveguide attenuator - (a) S_{21} magnitude, (b) S_{21} phase

Conclusion

This paper has presented a new W-Band bidirectional frequency converter module, featuring a very high level of integration. The architecture and implementational details were presented, and obtained experimental results were shown. An example was shown where the W-Band frequency converter was used to frequency extend two VNAs to allow vector (magnitude and phase) S_{21} measurements in the $76\,\mathrm{GHz}$ to $81\,\mathrm{GHz}$ range.

Ongoing and future work is in place to fix minor issues present in the prototype design, following on from which, this frequency converter is to be integrated in large-scale testing setups for an automotive radar IC production line. The converter is also commercially available for purchase from EECL and is suitable for a wide array of potential applications, including VNA and spectrum analyzer frequency extenders, development of future 5G and 6G communication systems, and as a general-purpose W-Band frontend.

EECL's ongoing commitment to enabling advanced millimeter-wave research and development is reflected in the provision of accessible, high-performance solutions and consultancy services, tailored to the needs of both academic and industrial innovation.

ACKNOWLEDGMENT

The authors would like to thank Mark Hughes from Marki Microwave, Jennie Holmes from APC Technology Group, and Kevin Browne from Richardson RFPD for their support in obtaining the components needed to develop the prototype for this converter design.

REFERENCES

[1] C. Waldschmidt, J. Hasch, and W. Menzel, "Automotive radar — from first efforts to future systems," *IEEE Journal of Microwaves*, vol. 1, no. 1, pp. 135–148, Jan. 2021, ISSN: 2692-8388. DOI: 10.1109/JMW.2020.3033616. Accessed: Apr. 2, 2025. [Online]. Available: https://ieeexplore.ieee.org/document/9318758/.

[2] G. R. MacCartney and T. S. Rappaport, "73 GHz millimeter wave propagation measurements for outdoor urban mobile and backhaul communications in new york city," in *2014 IEEE International Conference on Communications (ICC)*, ISSN: 1938-1883, Jun. 2014, pp. 4862–4867. DOI: 10.1109/ICC.2014.6884090. Accessed: Apr. 3, 2025. [Online]. Available: https://ieeexplore.ieee.org/document/6884090.

[3] U. J. Lewark, J. Antes, J. Walheim, J. Timmermann, T. Zwick, and I. Kallfass, "Link budget analysis for future e-band gigabit satellite communication links (71–76 and 81–84 ghz)," *CEAS Space Journal*, vol. 4, no. 1, pp. 41–46, Jun. 2013, ISSN: 1868-2502, 1868-2510. DOI: 10.1007/s12567-013-0030-0. Accessed: Apr. 3, 2025. [Online]. Available: http://link.springer.com/10.1007/s12567-013-0030-0.

[4] A. Yonamine, M. Kubota, O. Baba, K. Tsukashima, T. Tokumitsu, and Y. Hasegawa, "Development of e-band transmitter chipset using wafer level chip size package technology,"

[5] S. S. Cahill, E. A. Sanjuan, and D. Regev, "Scaling quad-flat no-leads package performance to e-band frequencies," in *2013 IEEE International Conference on Microwaves, Communications, Antennas and Electronic Systems (COMCAS 2013)*, Oct. 2013, pp. 1–5. DOI: 10.1109/COMCAS.2013.6685275. Accessed: Mar. 24, 2025. [Online]. Available: https://ieeexplore.ieee.org/document/6685275.

[6] M. Lippoldt, "Bond-wire impedance compensation for millimeter-wave chip interconnects." Accessed: Apr. 7, 2025. [Online]. Available: https://www.semanticscholar.org/paper/Bond-Wire-Impedance-Compensation-for-Chip-Lippoldt/2ce0b54053f5dd634682b4e84c4d6053ca3cf8cc.

[7] J. P. Dunsmore, *Handbook of Microwave Component Measurements: with Advanced VNA Techniques*, 1st ed. Wiley, Jul. 7, 2020, ISBN: 978-1-119-47713-6 978-1-119-47716-7. DOI: 10.1002/9781119477167. Accessed: Apr. 1, 2025. [Online]. Available: https://onlinelibrary.wiley.com/doi/book/10.1002/9781119477167.